

The First Hyper-Luminous Infrared Galaxy Discovered by WISE

Peter R. M. Eisenhardt¹, Jingwen Wu^{1,2}, Chao-Wei Tsai³, Roberto Assef^{1,2}, Dominic Benford⁴, Andrew Blain⁵, Carrie Bridge⁶, J. J. Condon⁷, Michael C. Cushing⁸, Roc Cutri³, Neal J. Evans II⁹, Chris Gelino³, Roger L. Griffith³, Carl J. Grillmair³, Tom Jarrett³, Carol J. Lonsdale⁷, Frank J. Masci³, Brian S. Mason⁷, Sara Petty¹⁰, Jack Sayers⁶, S. Adam Stanford¹¹, Daniel Stern¹, Edward L. Wright¹⁰, Lin Yan³

ABSTRACT

We report the discovery by the Wide-field Infrared Survey Explorer of the $z = 2.452$ source WISE J181417.29+341224.9, the first hyperluminous source found in the WISE survey. WISE 1814+3412 is also the prototype for an all-sky sample of ~ 1000 extremely luminous “W1W2-dropouts” (sources faint or undetected by WISE at 3.4 and 4.6 μm and well detected at 12 or 22 μm). The WISE data and a 350 μm detection give a minimum bolometric luminosity of $3.7 \times 10^{13} L_{\odot}$, with $\sim 10^{14} L_{\odot}$ plausible. Followup images reveal four nearby sources: a QSO and two Lyman Break Galaxies (LBGs) at $z = 2.45$, and an M dwarf star. The brighter LBG dominates the bolometric emission. Gravitational lensing is unlikely given the source locations and their different spectra and colors. The dominant LBG spectrum indicates a star formation rate $\sim 300 M_{\odot} \text{yr}^{-1}$, accounting for $\lesssim 10\%$ of the bolometric luminosity. Strong 22 μm emission relative to 350 μm implies that warm dust contributes significantly to the luminosity, while cooler dust normally associated with starbursts is constrained by an upper limit at 1.1 mm.

¹Jet Propulsion Laboratory, California Institute of Technology, MS 169-327, 4800 Oak Grove Drive, Pasadena, CA 91109 [e-mail: Peter.R.Eisenhardt@jpl.nasa.gov]

²NASA Postdoctoral Program Fellow

³Infrared Processing and Analysis Center, California Institute of Technology, Pasadena, CA 91125

⁴NASA Goddard Space Flight Center, Greenbelt, MD 20771

⁵Department of Physics & Astronomy, University of Leicester, Leicester, LE1 7RH, United Kingdom

⁶Division of Physics, Math and Astronomy, California Institute of Technology, Pasadena, CA 91125

⁷National Radio Astronomy Observatory, 520 Edgemont Road, Charlottesville, VA 22903

⁸University of Toledo, Toledo, OH 43606

⁹Department of Astronomy, University of Texas, Austin, TX 78712

¹⁰University of California, Los Angeles, CA 90095

¹¹University of California, Davis, CA 95616

Radio emission is $\sim 10\times$ above the far-infrared/radio correlation, indicating an active galactic nucleus is present. An obscured AGN combined with starburst and evolved stellar components can account for the observations. If the black hole mass follows the local M_{BH} -bulge mass relation, the implied Eddington ratio is $\gtrsim 4$. WISE 1814+3412 may be a heavily obscured object where the peak AGN activity occurred prior to the peak era of star formation.

Subject headings: galaxies: individual (WISE J181417.29+341224.9)

1. Introduction

The Wide-field Infrared Survey Explorer (WISE) launched on 2009 Dec. 14, and began surveying the sky on 2010 Jan. 14, completing its first full coverage in July 2010. WISE achieves 5σ point source sensitivities of better than 0.08, 0.11, 1, and 6 mJy at 3.4, 4.6, 12 and 22 μm (hereafter referred to as W1, W2, W3, and W4) in a single coverage on the ecliptic, consisting of 8 or more exposures at each sky location (Wright et al. 2010). Sensitivity improves away from the ecliptic due to denser exposure overlap and lower zodiacal background. The survey continued in W1 and W2 after the cryogen was exhausted at the end of Sept. 2010, and concluded 2011 Feb. 1, having achieved two complete sky coverages in these two bands. The WISE all-sky data release was issued on 2012 Mar. 14¹.

The primary science objectives for WISE are to identify the coldest and nearest brown dwarfs to the Sun (see e.g., Mainzer et al. 2011a; Cushing et al. 2011; Kirkpatrick et al. 2011), and the most luminous, dusty, forming galaxies (Ultra-luminous Infrared Galaxies or ULIRGs). With regard to the most luminous objects, the dominant sources of energy production in the Universe are fusion in stars and gravitational accretion onto super-massive black holes. The tight correlation between the masses of super-massive black holes at the centers of galaxies, and the masses of the stellar bulges in these galaxies (Magorrian et al. 1998; Ferrarese & Merritt 2000; Gebhardt et al. 2000), implies the two formation processes are intimately connected. Bulge stellar populations are old and quiescent today, and so must have formed in the distant past, when the cosmic star formation rate was much higher (e.g., Hopkins 2004). Similarly the peak era of accretion onto super-massive black holes was at redshifts $z \sim 2$, when luminous quasars were common (e.g., Richards et al. 2006a; Assef et al. 2011). There is substantial evidence that dust absorbs much of the UV/optical luminosity generated by the formation of massive galaxies and their central black holes at $z > 1$ (e.g., Blain et al. 2004; Floc'h et al. 2005; Stern et al. 2005; Hickox et al. 2007). The dust is heated in the process, and most of the luminosity emerges at IR wavelengths, creating a ULIRG.

The most extreme examples of ULIRGs are therefore likely associated with the major formation events of the most massive galaxies. Such objects should appear in the sensitive infrared all-sky

¹<http://wise2.ipac.caltech.edu/docs/release/allsky>

WISE survey, and may be missed in surveys with substantially smaller areas by e.g., *Spitzer* and *Herschel*. Here we report on WISE J181417.29+341224.9 (hereafter WISE 1814+3412), the first hyper-luminous infrared galaxy ($L_{\text{IR}} > 10^{13} L_{\odot}$) discovered by WISE.

Magnitudes are converted to flux densities using zeropoint values of 3631 Jy for the AB system g' and r' bands. Other magnitudes are on the Vega system, using zeropoints of 1594 and 666.7 Jy for the 2MASS system J and K_s bands; 280.9 and 179.7 Jy for *Spitzer* IRAC [3.6] and [4.5]; and 306.7, 170.7, 29.04 & 8.284 Jy for WISE W1 through W4 respectively (Wright et al. 2010). Luminosities are calculated assuming $\Omega_M = 0.3$, $\Omega_{\Lambda} = 0.7$, and $H_0 = 70 \text{ km s}^{-1} \text{Mpc}^{-1}$.

2. Selection Criteria and Followup Observations

Early searches for the most luminous galaxies with WISE data included the investigation of outlier populations, among them objects which were only well detected in W3 and W4, including WISE 1814+3412. This approach proved highly successful (Figure 1), leading to a variety of followup programs now underway on sources which are much fainter in W1 ($3.4 \mu\text{m}$) and W2 ($4.6 \mu\text{m}$) than W3 ($12 \mu\text{m}$) or W4 ($22 \mu\text{m}$). The selection criteria for these “W1W2-dropouts” are $W1 > 17.4$ ($< 34 \mu\text{Jy}$), and either: a) $W4 < 7.7$ ($> 6.9 \text{ mJy}$) and $W2 - W4 > 8.2$; or b) $W3 < 10.6$ ($> 1.7 \text{ mJy}$) and $W2 - W3 > 5.3$. W1W2-dropouts must also have at least 7 individual WISE exposures available for measurement in W3 or W4, be more than 30° from the Galactic center and 10° from the Galactic plane, be free of artifacts flagged by the WISE pipeline, not be associated with known asteroids (including asteroids discovered by WISE; Mainzer et al. 2011b), and finally pass a series of visual inspections of both the individual exposures and coadded images for evidence of spurious sources. Figure 1 illustrates the rarity of W1W2-dropouts in WISE color-color space. The sources have a surface density $\lesssim 0.03 \text{ deg}^{-2}$, or $< 10^{-5}$ that of WISE sources in general. Figure 1 also shows the distribution of the 143 redshifts currently known for the sample. Over 60% of W1W2-dropouts are at $z > 1.6$, with most of the low redshift population optically bright, as noted by Bridge et al. (2012).

WISE 1814+3412 satisfies all these selection criteria, and was initially identified in 2010 May using similar criteria and available data. Of the 37 sources which satisfied the criteria at the time, WISE 1814+3412 was the brightest in W4. Figure 2 shows cutouts of images in the four WISE bands of WISE 1814+3412, and Table 1 gives W3 and W4 PSF fitted photometry for the source. In the two shorter bands the 2σ limit for W1 is formally > 18.67 ($< 11 \mu\text{Jy}$) although magnitudes at these levels appear to underestimate the true flux density, while there is a marginal detection at $W2 = 17.17 \pm 0.49$ ($23 \pm 11 \mu\text{Jy}$).

2.1. Images at Other Wavelengths

Followup imaging observations of WISE 1814+3412 have been carried out from optical to radio wavelengths, with results summarized in Table 1. Details of these observations follow.

2.1.1. Optical Imaging

Optical imaging of WISE 1814+3412 using g' and r' filters was obtained on UT 2011 May 28 with the Mosaic-1.1 Imager (Sawyer et al. 2010) on the KPNO 3.8 m diameter² Mayall telescope. The pixel size was $0''.26$ at the center of the CCD mosaic, declining to $0''.245$ at the edge of the $36'$ field. Three dithered 500 s exposures in the two filters were obtained in clear conditions with sub-arcsecond seeing. Pipeline processed stacked images resampled onto uniform $0''.25$ pixels were retrieved from the NOAO Science Archive, yielding a FWHM image size of $0''.75$ in g' and $0''.70$ in r' . Small ($\sim 0''.2$) astrometric offsets were made to the image world coordinate system (WCS) to remove any differences with 2MASS catalog positions of objects in the field. Because the WISE 1814+3412 field is not included in the SDSS, flux calibration was obtained using several short (30 s) observations in the two filters of another W12drop with SDSS coverage 10° away. These were immediately followed by 30 s exposures of WISE 1814+3412 in g' , then by full depth 500 s exposures of WISE 1814+3412 in r' , and finally by full depth 500 s exposures of WISE 1814+3412 in g' . All observations of the two W12drop fields were at an airmass of 1.04 or less. No significant change in zero point was detected between the 30 s and 500 s g' exposures on WISE 1814+3412.

The lower left panel of Figure 2 shows a $2' \times 2'$ region of the reduced r' image centered on WISE 1814+3412, and the upper left panel of Figure 3 shows a zoomed in view of the g' image covering $20'' \times 20''$. Several objects are apparent near the WISE 1814+3412 coordinates, with the closest being a somewhat extended source (labeled “A” in the upper left panel of Figure 3), two unresolved sources (“B” and “C”) to the north, a fainter source (“D”) a few arcsec to the southwest, and two other faint sources farther to the southwest and east. These sources are also seen in the r' image. Components A, B, C, and D were also seen in optical images obtained on UT 2010 June 14 at Palomar Observatory using the Hale 5.08 m telescope with the Large Format Camera (Simcoe et al. 2000) at prime focus. The Palomar images were used to position spectroscopic slits as described in § 2.2, but because of their relatively poor image quality and non-photometric conditions, are not further discussed here.

Because of the close proximity of source B to A and the fact that source A is extended, the optical photometry for source A reported in Table 1 is from a $7''.5$ diameter aperture in an image in which sources B and C have been PSF subtracted. The optical photometry for source B in Table 1 is from PSF fitting.

²Although generally referred to as the KPNO 4m telescope, the clear aperture diameter of the Mayall telescope is 3.797m, as documented at http://www-kpno.kpno.noao.edu/kpno-misc/mayall_params.html

2.1.2. Near-IR Imaging

WISE 1814+3412 was targeted for followup in K_s with the NIRC2 camera on the Keck II telescope using laser guide star adaptive optics (Wizinowich et al. 2006) on UT 2010 July 1, and in J on UT 2011 July 20. A total of 30 minutes of integration were obtained in K_s using dithered 1 minute exposures, and 18 minutes in J using 2 minute exposures, with a pixel scale of $0''.0397$ giving a $40''$ field. The K_s data were obtained under photometric conditions and $0''.35$ seeing, while for J the seeing was $> 1''$ and the sky was cloudy at the end of the night. An $R = 15.5$ star $33''$ from WISE 1814+3412 was used to provide tip-tilt correction.

Each individual image was sky subtracted using a median of the 4 preceding and 4 following images. The sky-subtracted images were roughly registered using the recorded position of the AO tip-tilt sensor stage, and then fine tuned by minimizing their residuals relative to the first image. The final mosaic was formed from the median of aligned images. Photometric calibration was achieved using several well exposed stars in common with the wider field Palomar/WIRC data described below, but because these exhibited an rms dispersion of 0.2 mag, that dispersion was imposed as a minimum photometric error. Astrometric calibration was achieved using sources in common with the optical r' image which had been registered to the 2MASS frame (§ 2.1.1). The upper right panel of Figure 3 shows the central $20'' \times 20''$ of the resulting K_s image. Components A, B, C, and D are detected in K_s , while in J , component A is faint and D is undetected. In both images component A is clearly extended relative to components B and C. Photometry was measured in a 50 pixel ($1''.99$) diameter aperture for component A and a 20 pixel ($0''.79$) diameter aperture for component B, centered on the peak of each component.

A K_s image covering $8'.7$ on the WISE 1814+3412 field was obtained on UT 2010 July 27 and in J on 2011 Sept. 17 with the Wide-field Infrared Camera (WIRC; Wilson et al. 2003) at Palomar Observatory using the Hale 5.08 m telescope. For both images the seeing was sub-arcsecond and the pixel size was $0''.25$. The total integration time was 18 minutes for K_s and 5 minutes for J , with 1 minute per dither. The data were flatfielded and coregistered, and calibrated to 2MASS. Although WISE 1814+3412 was only faintly detected in K_s and not at all in J in these data, the WIRC images enabled the photometric calibration of the deeper NIRC2 images to be tied to 2MASS.

2.1.3. Spitzer

WISE 1814+3412 was observed by *Spitzer* at [3.6] and [4.5] on 2010 July 22 using Director's Discretionary Time (Program # 549). The source was observed with the $1''.2$ pixels and $5'$ field of each IRAC band using twelve exposures each 100 s long, employing the medium scale Reuleaux dither pattern. Figure 2 shows the *Spitzer* pipeline post-BCD processed image of WISE 1814+3412 at $3.6 \mu\text{m}$, which is resampled onto $0''.6$ pixels, while Figure 3 shows the $4.5 \mu\text{m}$ image.

The multiple components seen in Figure 3 are present in the *Spitzer* data, with the relative

prominence of component A increasing at longer wavelengths. Similar to the optical imaging (§ 2.1.1), the *Spitzer* photometry for source A reported in Table 1 is from a 12'' diameter aperture in an image in which sources B and C were PSF subtracted, while the photometry for source B is from PSF fitting. The [4.5] detection is consistent with the WISE W2 given above, while the [3.6] detection implies that the W1 2σ limit underestimates the true flux density. A minimum photometric error of 0.1 mag has been imposed on the *Spitzer* photometry.

2.1.4. Far-Infrared Data

WISE 1814+3412 is undetected by IRAS. Using SCANPI³, the 2σ upper limits are < 40 mJy at 12 and 25 μm , < 100 mJy at 60 μm , and < 600 mJy at 100 μm . These limits are consistent with the W3 and W4 detections of WISE 1814+3412.

2.1.5. Caltech Submillimeter Observatory Data

Continuum observations of WISE 1814+3412 at 350 μm were obtained on 2010 July 13 and 23, and at 450 μm on 2010 Sept. 12 and 13, using the Submillimeter High Angular Resolution Camera II (SHARC-II) at the 10.4 m telescope of the Caltech Submillimeter Observatory (CSO) at Mauna Kea, Hawaii (Dowell et al. 2003). SHARC-II uses a bolometer array with 32×12 pixels, resulting in a $2.59' \times 0.97'$ field of view. The beam sizes of SHARC-II at 350 and 450 μm are $8''.5$ and $10''.9$ respectively.

Atmospheric transmission at 350 μm and 450 μm is poor when the opacity at 225 GHz (τ_{225}) is > 0.07 . WISE 1814+3412 was observed near transit for 160 minutes at 350 μm with $\tau_{225} = 0.035 - 0.06$ and for 90 minutes at 450 μm with $\tau_{225} = 0.045$. The telescope was scanned in a Lissajous pattern that keeps the source within the FOV. The Dish Surface Optimization System (DSOS; Leong et al. 2006) was used to correct the dish surface figure for imperfections and gravitational deformations as the dish moves in elevation during observations.

The SHARC-II data were reduced using version 2.01-4 of the Comprehensive Reduction Utility for SHARC-II (CRUSH; Kovács 2006). Pointing was checked every 1-2 hours and corrected to $< 2''.0$ in altitude and $< 2''.5$ in azimuth using Uranus when available, and with a secondary calibrator, K3-50 (a massive star forming region close to WISE 1814+3412). The processed 350 μm image is shown in Figure 2. Flux calibration was obtained using Uranus. We derive a flux density at 350 μm of 33 ± 9 mJy for WISE 1814+3412. At 450 μm the detection was not significant, with a flux density of 15 ± 10 mJy. We report in Table 1 a 95% confidence upper limit of 35 mJy at 450 μm , based on the statistical methods described by Feldman & Cousins (1998).

³<http://irsa.ipac.caltech.edu/IRASdocs/scanpi>

WISE 1814+3412 was observed at 1.1 mm with the CSO using the Bolocam instrument for a total of ten hours on UT 2010 June 18 and 19. Bolocam is a large format camera with 144 detectors, an 8' FOV, and a 30'' FWHM (Haig et al. 2004). The telescope was scanned in a Lissajous pattern keeping the source in the FOV. Pointing was checked and corrected to 6'' using frequent observations of the nearby bright objects K3-50 and 3C345 following methods described in Sayers et al. (2009). Flux calibration, estimated to be accurate to $\simeq 10\%$ (Sandell 1994), was determined using K3-50. Atmospheric contributions to the signal were subtracted using a modified version of the algorithms described in Sayers et al. (2011, details in Wu et al. 2012). The atmospheric subtraction also attenuates astronomical signal, and to account for this, K3-50 was processed in an identical way prior to determining the flux calibration.

The 1.1 mm flux density at the location of WISE 1814+3412 is formally -0.8 mJy. The noise fluctuations in the map are Gaussian within our ability to measure them. Including the estimated confusion noise rms per beam of 0.6 mJy, the estimated total rms per beam at the location of WISE 1814+3412 is 1.6 mJy. Based on the statistical methods of Feldman & Cousins (1998), the corresponding 95% confidence upper limit is 2.4 mJy at 1.1 mm, as listed in Table 1.

2.1.6. Radio

WISE 1814+3412 was observed with 22 antennas of the D configuration of the Expanded Very Large Array (EVLA) on 2010 June 10. Observations were made simultaneously in two 128 MHz bands centered on 4.494 GHz (6.77 cm, “C-band low”) and 7.93 GHz (3.78 cm, “C-band high”) in order to obtain a spectral index. The on-source integration time was 29 minutes. The source J1759+2343 was used for phase calibration and 3C48 was used for flux calibration. The C-band data were calibrated and imaged using Common Astronomy Software Applications⁴ (CASA). The 4.494 GHz image has 39 μ Jy/beam rms noise in the 15.1'' \times 12.3'' beam (with major-axis PA = -42°), and the 7.93 GHz image has 67 μ Jy/beam noise with a 8.7'' \times 7.1'' beam at PA = -37° .

Source positions and flux densities were estimated from Gaussian fits made by the AIPS task IMFIT. An unresolved source coincident with WISE 1814+3412 to within the astrometric errors (i.e. ± 0.03 s in RA and $\pm 0''.5$ in dec) and a flux density of 560 ± 70 μ Jy was detected at 4.494 GHz (Figure 2). At 7.93 GHz, WISE 1814+3412 has a flux density of 350 ± 130 μ Jy, giving a spectral index $\alpha \approx 0.8$, where $F_\nu \propto \nu^{-\alpha}$. A second unresolved source was detected 4'' east and 39'' south of WISE 1814+3412 with flux densities of 790 ± 70 μ Jy at 4.494 GHz and 460 ± 120 μ Jy at 7.93 GHz ($\alpha \sim 1.0$). The counterpart to this second source at r' and [3.6] is indicated in Figure 2 with an arrow. Using the spectral indices to extrapolate the EVLA flux densities for the two sources to 1.4 GHz predicts 1.4 mJy for WISE 1814+3412 and 2.4 mJy for the southern source. The sum of these flux densities is consistent with the NRAO VLA Sky Survey (NVSS; Condon et al. 1998)

⁴<http://casa.nrao.edu/>

measurement of 3.4 ± 0.5 mJy, which is a blend of the two sources.

Observations of WISE 1814+3412 in the Ka band (26 – 40 GHz, or 9.7 mm at 32 GHz) were acquired with the Green Bank Telescope (GBT) on 2010 November 10 using the Caltech Continuum Backend (CCB). A total on-source integration time of 25 minutes was obtained from 38 useful one-minute “nod” (beam-switched) observations. The telescope pointing was corrected dynamically with reference to the bright nearby source 1814+4113. The flux calibration was established by an observation of 3C48, which was assumed to have a flux density at 32.0 GHz of 0.82 Jy, and a spectral index of $\alpha = 1.18$. This flux density is based on the 32 GHz brightness temperature measurement of Jupiter ($T_J = 146.6 \pm 0.75$ K; Hill et al. 2009). The data were reduced in publicly available IDL routines custom written to process GBT+CCB data, using the approach described in Mason et al. (2009). All four 3.5 GHz channels over the 26 to 40 GHz frequency band were averaged together to maximize the sensitivity, giving a 2σ upper limit of 175 μ Jy for WISE 1814+3412.

2.2. Optical Spectroscopy

We obtained the discovery spectrum revealing that WISE 1814+3412 was at $z = 2.452$ on UT 2010 May 12 with the dual-beam Low Resolution Imaging Spectrometer (LRIS; Oke et al. 1995) with its Atmospheric Dispersion Compensator (ADC) on the Keck I telescope. Two dithered 600 s exposures were obtained in clear conditions with sub-arcsecond seeing. The observations used the 1"5 wide longslit, the 6800 Å dichroic, the 400 ℓ mm⁻¹ grating on the red arm of the spectrograph (blazed at 8500 Å; resolving power $R \equiv \lambda/\Delta\lambda \sim 700$ for objects filling the slit), and the 400 ℓ mm⁻¹ grism on the blue arm of the spectrograph (blazed at 3400 Å; $R \sim 600$). An offset star 22"1 to the northwest was used to position the spectrograph slit on the WISE source, with a slit position angle (PA) of 143.6° so that the offset star remained in the slit.

Additional LRIS-ADC spectroscopy of WISE 1814+3412 and sources in its vicinity (§ 2.1.1, Figure 3) was obtained during UT 2010 July 13–15. These observations used the 1"5 wide longslit, the 5600 Å dichroic, the 600 ℓ mm⁻¹ blue grism (blazed at 4000 Å; $R \sim 1000$), and the same 400 ℓ mm⁻¹ red grating as used in May 2010. The nights were photometric. On UT 2010 July 14 two dithered 600 s exposures were obtained at a PA of 8.0° to simultaneously observe components A and B, and two dithered 600 s exposures were obtained at a PA of 12.0° to simultaneously observe components C and D. On UT 2010 July 15 two dithered 900 s exposures were obtained at a PA of 205.0° to simultaneously observe components B and D. In each case, the red arm exposure time was 60 s shorter than the 600 s or 900 s blue arm exposure time. The data were processed using standard procedures, and flux calibrated using observations of standard stars from Massey & Gronwall (1990). The reduced spectra are presented in Figure 4.

The upper left panel of Figure 4 shows the July 2010 spectrum of component A, which is of slightly higher quality than the May 2010 data. WISE 1814+3412 shows a typical Lyman-break galaxy (LBG) spectrum at redshift $z = 2.452$, with Ly α emission, a continuum break across the

emission line due to the Ly α forest, and several UV interstellar absorption lines. The spectrum shows no signs of high ionization, high equivalent width emission lines typical of AGN activity. For comparison, the LBG composite spectrum from Shapley et al. (2003) is shown directly below the component A spectrum in Figure 4. The May 2010 spectrum shows Ly α emission extending > 30 kpc to the southeast (PA 143.6 $^\circ$) of component A, making it a Ly α blob (Bridge et al. 2012).

The upper right panel of Figure 4 shows the combined spectrum from the two PA’s covering component B, which has a much redder optical spectrum than the other components, and appears to be an early-type M-dwarf star. The colors $g' - r' = 1.48$, $J - [4.5] = 0.95$, $K_s - [3.6] = 0.11$, and $[3.6] - [4.5] = 0.17$ support this interpretation (Bochanski et al. 2007; Patten et al. 2006).

The lower left panel of Figure 4 shows the spectrum of component C. This source is a typical broad-lined (i.e., unobscured or Type 1) quasar at the same redshift as WISE 1814+3412. Self-absorption is clearly evident in the Ly α , Si IV and C IV transitions.

The lower right panel of Figure 4 shows the spectrum of component D. The spectrum has a relatively flat (in F_ν) continuum, with a broad absorption and continuum break at approximately the same wavelength as Ly α at $z \sim 2.45$. Several interstellar absorption lines are evident that match this interpretation, implying that component D is at the same redshift as WISE 1814+3412.

2.3. Astrometry

Table 2 gives the measured positions for WISE 1814+3412 components A, B, C, and D, when the different components are detected. Only the seconds of right ascension and arcseconds of declination of the coordinates for components B, C, and D are listed. For the WISE, CSO, and radio data, only a single component is detected. A minimum uncertainty of 0''.2 is assumed to account for systematic uncertainties with respect to an absolute reference frame, which is larger than the internal measurement errors for the optical, near-IR, and *Spitzer* data.

As can be seen in the lower panels of Figure 3, the positions of component A and of the single detected component in the longer wavelength data are in agreement, within the errors.⁵ With a reduced chi-squared value of 0.984 for the profile fit to a point source in the WISE data, WISE 1814+3412 is unresolved. In W3, with a reduced chi-squared of 0.98, the source FWHM is $< 1''$, while in W4 the reduced chi-squared of 1.09 corresponds to a FWHM $< 6''$. The separations of 5''.2 between component A and C, and of 3''.8 between component A and D, are large compared to the

⁵The WISE catalog coordinates listed in Table 2 are in agreement with the coordinates for component A in other bands, and have a systematic uncertainty with respect to 2MASS of $< 0''.2$. The world coordinate system (WCS) in WISE image tiles deviates slightly but systematically from the catalog coordinates for sources in the tile, with the catalog coordinates being correct. For the image tile containing WISE 1814+3412 this offset causes sources to appear 0''.68 East and 1''.10 South of their overlaid catalog coordinates, and we have adjusted the WISE image WCS to correct for this in the bottom center panel of Figure 3.

uncertainties in the WISE position, or in the 4.5 GHz (C-band low) position. We therefore conclude that component A at $z = 2.452$ is predominantly responsible for the flux from the single component seen in the longer wavelength data, and hereafter refer to component A as WISE 1814+3412 unless otherwise indicated.

However, Figure 3 suggests that there is a noticeable shift in the position of component A with respect to component C in the highest resolution images. Component A lies essentially due south of component C in the K_s and *Spitzer* images, but in the optical images component A is shifted $\approx 0''.5$ to the east, or 4 kpc at $z = 2.452$. As a point source and $z = 2.45$ quasar, component C is almost certainly at a fixed position in all images, so we believe this shift in the component A optical centroid position with respect to the K_s and *Spitzer* positions to be real. Because the optical spectrum and photometry suggest appreciable extinction is present (§3.3), we consider it most likely that the K_s and *Spitzer* positions of component A are coincident with the WISE and radio positions, with the optical centroid of component A slightly displaced from these.

3. Analysis

Figure 5 compares WISE and *Spitzer* photometry for WISE 1814+3412 to other unusually red objects redshifted to $z = 2.452$ and normalized at $22 \mu\text{m}$. These include the well known ULIRGs Arp 220 and Mrk 231; the extremely red $z = 0.058$ IRAS source 08572+3915; the $z = 1.293$ source SST24 J1428+3541 (Desai et al. 2006), which is the brightest $24 \mu\text{m}$ source (10.55 mJy) among mid-IR sources with faint optical counterparts in the 8 deg^2 Boötes field; the $z = 2.40$ source N2_08 (SWIRE J164216.93+410127.8), which is the most luminous obscured QSO from the sample of Polletta et al. (2008); and source A10 (SWIRE J103916.79+585657.9) from Weedman et al. (2006), which does not have a measured redshift and is among the reddest sources found in the SWIRE survey. None of these are as extreme as WISE 1814+3412 in the W2 to W3 range (4.6 to $12 \mu\text{m}$). Wu et al. (2012) show that W1W2-dropouts readily satisfy the $R - [24] \geq 14$ criterion for “DOGs” (dust obscured galaxies, Dey et al. 2008). Dey et al. (2008) suggest the $24 \mu\text{m}$ emission in the brighter DOGs arises from warm dust heated by an AGN, and since the $24 \mu\text{m}$ flux density limit for DOGs is $\sim 20\times$ fainter than for W1W2-dropouts, AGN might be expected to play an important role in W1W2-dropouts.

3.1. SED Modeling

Figure 6 plots the observed photometry for WISE 1814+3412. The detections in W3 ($12 \mu\text{m}$), W4 ($22 \mu\text{m}$), and $350 \mu\text{m}$ and the upper limits at $450 \mu\text{m}$ and 1.1 mm imply the luminosity (§ 3.2) is dominated by emission from warm dust, possibly heated by an AGN. The EVLA detections show an AGN is present (§ 3.6). The similarity of the WISE 1814+3412 optical spectrum to a Lyman Break Galaxy (§ 2.2) implies that active star formation is underway, as discussed in § 3.3.

Motivated by these components, in Figure 6 we show an example fit to the optical, near-IR, *Spitzer* and WISE photometry for WISE 1814+3412 using starburst and evolved stellar population templates from Assef et al. (2010), and a reddened Type 1 AGN template from Richards et al. (2006b).⁶ As in Assef et al. (2010), the reddening is assumed to follow an SMC-like extinction curve (Gordon & Clayton 1998) for $\lambda < 3300 \text{ \AA}$ and a Galactic extinction curve (Cardelli et al. 1989) at longer wavelengths, in both cases with $R_V = 3.1$. The resultant AGN template extinctions in the rest frame are $E(B - V) = 15.6 \pm 1.4$ or $A_V = 48 \pm 4$, corresponding to $A_{W3} = 2.7 \pm 0.2$ and $A_{W4} = 0.98 \pm 0.09$ in the observed frame. Because the Richards et al. (2006b) template does not extend to $350 \mu\text{m}$ ($100 \mu\text{m}$ rest), this reddened Type 1 AGN component was *not* fit to the submillimeter photometry, but with a small extrapolation it nevertheless provides a good match to those data. The cyan line in Figure 6 shows a 490 K blackbody fit to the W3 ($12 \mu\text{m}$) and W4 ($22 \mu\text{m}$) photometry, while the magenta line shows a modified (i.e., with dust emissivity $\propto \nu^{1.5}$) 45 K blackbody fit to the $350 \mu\text{m}$ flux density and the upper limit at 1.1 mm. Finally, the dotted line shows a radio spectral index $\alpha = 0.8$ fit to the EVLA data (§ 2.1.6). We consider each of these components in more detail below.

3.2. Luminosity Estimates

We obtain a lower limit of $L_{\text{bol}} > 3.7 \times 10^{13} L_{\odot}$ for the bolometric luminosity of WISE 1814+3412 by assuming the SED is given by two power laws connecting the observed flux densities at W3, W4, and $350 \mu\text{m}$, with no luminosity at shorter or longer wavelengths, as shown by the light dashed lines in Figure 6. The luminosity can also be estimated by integrating over the best-fit SED templates of § 3.1, which are dominated by the dust-reddened AGN component, extending the latter beyond $350 \mu\text{m}$ via a $F_{\nu} \propto \nu^{3.5}$ power law. The details of this extrapolation are not significant as nearly all of the flux is already contained in the reddened AGN template. This approach yields a bolometric luminosity estimate of $9.2 \pm 1.0 \times 10^{13} L_{\odot}$, of which $7.2 \pm 0.8 \times 10^{11} L_{\odot}$ ($< 1\%$) is from the stellar components. From the upper limit to the IRAS $60 \mu\text{m}$ flux density (§2.1.4) plotted in Figure 6, the luminosity is unlikely to be a factor of two higher.

3.2.1. Lensing

Luminosities approaching $10^{14} L_{\odot}$ inevitably lead to suspicions that WISE 1814+3412 is gravitationally lensed, as is true for sources such as IRAS FSC10214+4724 (e.g., Eisenhardt et al. 1996) and APM 08279+5255 (e.g., Ibata et al. 1999). However, Figures 3 and 4 show lensing is unlikely to be a significant factor for WISE 1814+3412. Although there are multiple components at the same redshift (A, C, D), their SEDs and spectra have different characteristics. The obvious candidate

⁶Due to its longer wavelength range, the Richards et al. (2006b) AGN template was used rather than that from Assef et al. (2010), although the fit is qualitatively identical with either template.

for a foreground lens is component B, but this appears to be a Galactic M dwarf star (§ 2.2) rather than a massive galaxy at intermediate redshift. The extended K_s emission at $\text{PA} \sim 140^\circ$ around component A seen in Figure 3 is unlikely to come from a foreground lensing galaxy, as it coincides with extended $z = 2.452$ Ly α emission at the same PA (§ 2.2). Therefore the large luminosity of WISE 1814+3412 appears to be intrinsic.

3.3. Starburst Component

The spectrum of WISE 1814+3412 is typical of an LBG (§ 2.2), implying active star formation directly detected in the rest-frame UV. Assuming no UV extinction, the star formation rate (SFR) from the average L_ν of the starburst component of our fit (§ 3.1) over rest 1500 - 2800 Å and equation (1) of Kennicutt (1998) is $\sim 50 M_\odot \text{yr}^{-1}$ for a Salpeter initial mass function (IMF) from 0.1 to 100 M_\odot , or $\sim 30 M_\odot \text{yr}^{-1}$ for a Chabrier (2003) IMF.

However, even UV-selected LBG galaxies show evidence for extinction (Shapley et al. 2003). We estimate the extinction in WISE 1814+3412 by comparing the observed $g' - r' = 0.34$ color (AB system) to the color expected from Bruzual & Charlot (2003) models, using the “Ez_Gal” web tool⁷. Continuously star-forming models with Salpeter and Chabrier IMF’s, solar and 0.4 solar metallicities, and ages of 0.1 to 0.4 Gyr were considered. The model $g' - r'$ colors range from 0.01 for solar metallicity models which have been forming stars for 0.4 Gyr, to -0.12 for 0.1 Gyr models with 0.4 solar metallicity, and do not change substantially between the two IMF’s. Using the reddening law from equation (4) of Calzetti et al. (2000), these colors imply extinction at 0.16 μm ranging from 2.00 to 2.75 mag. The corresponding corrected SFR values are $\sim 300(180)$ to 600(350) $M_\odot \text{yr}^{-1}$ for a Salpeter (Chabrier) IMF. Higher SFR values are possible if some is completely obscured in the UV.

3.4. Stellar Component

The stellar mass can be estimated from the observed 17.13 magnitude at 4.5 μm , the longest wavelength in the SED dominated by the stellar component (Figure 6). The starburst component of the template fit (§ 3.1) falls well below the observed K_s , [3.6] and [4.5] SED, requiring a significant contribution from older stars, as represented by the Sbc template.

An upper limit for the plausible stellar mass can be obtained using the Bruzual & Charlot (2003) models by assuming that the observed [4.5] flux density is from stars formed in a 0.1 Gyr burst at $z = 10$ (i.e. 2 Gyr before they are observed at $z = 2.452$) with a Salpeter IMF and solar metallicity. This model predicts $M/L = 0.51$ in rest K , much higher than the ~ 0.1 value typical

⁷<http://www.mancone.net/ezgal/model>

of the starburst models considered in § 3.3, but still well below the value of ~ 1 typical of present day galaxies (Bell et al. 2003). Allowing for extinction of 0.34 mag at [4.5] corresponding to the upper end of the range inferred in § 3.3 from the observed vs. model $g' - r'$ colors, this approach gives an upper limit to the stellar mass of $5.8 \times 10^{11} M_{\odot}$. While larger extinction values and hence masses are of course possible, this value is already many times the stellar mass of a field L* galaxy today ($\sim 5 \times 10^{10} M_{\odot}$; e.g. Baldry et al. 2008).

A lower limit can be obtained assuming that all the observed [4.5] light comes from one of the starburst models considered in § 3.3. The smallest stellar mass obtained with this approach is $4.1 \times 10^{10} M_{\odot}$, for a 0.1 Gyr old burst with solar metallicity and a Chabrier IMF. A more plausible model with equal contributions to the [4.5] luminosity from a starburst and an evolved stellar population, and with a more typical extinction at [4.5] of 0.3 mag, yields a stellar mass of $3.6(2.0) \times 10^{11} M_{\odot}$, for a Salpeter/Chabrier IMF.

3.5. Dust Component

The prominent emission of WISE 1814+3412 in W3 and W4 implies a significant contribution from warm dust. Fitting a blackbody to the W3 to W4 flux density ratio of 0.13 at $z = 2.452$ yields a temperature of ~ 490 K (cyan curve in Figure 6). Of course a range of temperatures is needed to account for all the data, but a modified blackbody (with $F_{\nu} \propto \nu^{1.5} B_{\nu}$) fit to the W4 to $350\mu\text{m}$ ratio of 0.44 also implies warm dust (~ 170 K). The scale of the warm dust is substantial: 30 to 250 pc for the radius of a spherical blackbody with $L_{\text{bol}} = 9 \times 10^{13} L_{\odot}$ and temperatures of 490 to 170 K. Using equation (1) of Calzetti et al. (2000) with $F_{350}/(1+z)$ as the rest $100 \mu\text{m}$ flux density, the warm dust mass is $\gtrsim 10^7 M_{\odot}$. The gas mass is $\gtrsim 10^9 M_{\odot}$ for the Milky Way gas to dust ratio, but could be up to $\sim 10^{11} M_{\odot}$ using the gas to dust ratio in AGN (Maiolino et al. 2001).

In contrast, the ratio of the $350 \mu\text{m}$ to 1.1 mm flux density is greater than 13.75, which means that dust at the cooler temperatures associated with sub-mm galaxies (~ 35 K; e.g. Kovács et al. 2006) plays a smaller role in the bolometric luminosity of this source. Wu et al. (2012) find that this predominance of warm dust is a characteristic of W1W2-dropouts, using CSO observations of 26 sources. For WISE 1814+3412, dust cooler than 45 K with $F_{\nu} \propto \nu^{1.5} B_{\nu}$ normalized to the observed $350 \mu\text{m}$ flux density would exceed the 2.4 mJy 95% confidence upper limit at 1.1 mm (magenta curve in Figure 6).

Nevertheless it seems likely that WISE 1814+3412 contains a cooler dust component. Figure 3 (see also §2.3) shows the rest UV emission from component A is displaced from the rest optical and near-IR by ~ 4 kpc, suggesting extinction on a much larger scale than the warm dust. The L_{IR} expected from a $\sim 300 M_{\odot}\text{yr}^{-1}$ SFR (§3.3) is $\sim 2 \times 10^{12} L_{\odot}$ (Kennicutt 1998). Dust with this luminosity at 35 K with $F_{\nu} \propto \nu^{1.5} B_{\nu}$ would contribute more than half the $350 \mu\text{m}$ flux density and just satisfy the 1.1 mm limit, and have a mass of $\sim 2.5 \times 10^8 M_{\odot}$.

3.6. Radio Source

The rest 1.4 GHz luminosity is $\sim 5 \times 10^{25} \text{ W Hz}^{-1}$, and the ratio of rest 5 GHz (\sim observed 1.4 GHz) to rest 4400 Å (\sim observed J) flux densities is ~ 200 . Both metrics qualify WISE 1814+3412 as radio-loud (Stern et al. 2000). If free-free emission from HII regions associated with star formation were present in WISE 1814+3412 at the level seen in M82 (Condon 1992, Figure 1), the Ka band upper limit of 175 μJy limit (§ 2.1.6) should have been exceeded, but the limit is consistent with the 115 μJy flux density expected from extrapolating the EVLA observations. This argues against star formation dominating the energetics of WISE 1814+3412.

Using the template SED fit and radio properties to estimate the $z = 2.452$ rest frame flux densities at 60 μm , 100 μm and 1.4 GHz (90, 33 mJy, and 3.9 mJy respectively), we obtain $q = 1.36$ from equations 14 and 15 of Condon (1992). This is $\sim 10\times$ more radio loud than the normal value of 2.4 ± 0.24 (Ivison et al. 2010), again implying the presence of an AGN. We conclude the radio emission in WISE 1814+3412 is due to AGN activity, rather than to star formation.

3.7. AGN Component

Over 99% of the bolometric luminosity in the template fit to the SED comes from the reddened Type 1 AGN component (§3.2), although there are no AGN features in the component A spectrum (§2.2). Wu et al. (2012) show W1W2-dropouts exhibit a range of rest-UV spectra, from an absence of any AGN signatures to the presence of broad lines, with most showing AGN features. The most direct evidence for an AGN in WISE 1814+3412 comes from the radio emission, which is above the radio-IR correlation (§3.6). Since the SED modeling finds $A_V = 48$ mag, corresponding to ~ 200 mag extinction in the rest UV, it is not surprising that AGN features such as broad lines and UV continuum from close to the black hole are absent from the spectrum. The corresponding proton column to the AGN is $\sim 10^{23} \text{ cm}^{-2}$ for Milky Way reddening (Bohlin et al. 1978), but up to $\sim 10^{25} \text{ cm}^{-2}$ (i.e. Compton-thick) using gas to dust ratios for AGN (Maiolino et al. 2001). If the source hosts an extremely luminous and obscured AGN, data from approved XMM-Newton and NuSTAR (Harrison et al. 2010) programs should reveal a hard X-ray spectrum, with few photons below rest-frame 10 keV.

Deep spectropolarimetry might detect AGN features. Such work has been done for example for $z \sim 2$ radio galaxies with similar optical brightness, with exposures typically needing most of a Keck night per target (Dey et al. 1996; Cimatti et al. 1998), and IRAS FSC10214+4724 (Goodrich et al. 1996, optically much brighter than WISE 1814+3412). All these objects show high ionization, narrow emission lines in their unpolarized spectra, and the lack of such features in WISE 1814+3412 is interesting, since typically they come from regions on a kpc scale (e.g., Bennert et al. 2002). This suggests that either the narrow line region is more compact for this source and/or that obscuring material is present on larger scales than the torus (e.g., Brand et al. 2007). The shift between the rest-UV and optical continuum (Figure 3) provides support for this idea.

If the luminosity in WISE 1814+3412 is due primarily to accretion onto a super massive black hole (SMBH), the SMBH mass for the template fit AGN luminosity is $2.8 \times 10^9 (L_{\text{Edd}}/L_{\text{bol}}) M_{\odot}$, where $(L_{\text{bol}}/L_{\text{Edd}})$ is the Eddington ratio. The dust sublimation radius is ~ 7 pc, and the outer radius of the dust torus is expected to be no more than $30\times$ the sublimation radius (Nenkova et al. 2008). This size is consistent with the range discussed in §3.5, but larger scale dust would be needed to obscure a kpc scale narrow line region.

4. Summary and Discussion

With a minimum bolometric luminosity of $3.7 \times 10^{13} L_{\odot}$, and more likely $L_{\text{bol}} \sim 9 \times 10^{13} L_{\odot}$, WISE 1814+3412 easily qualifies as a hyper-luminous infrared galaxy, the first identified by WISE. Its W4 ($22 \mu\text{m}$) flux density and redshift exceed that of the brightest $24 \mu\text{m}$ source DOG in the 8 deg^2 Boötes field (SST24 J1428+3541; Desai et al. 2006), giving it a rest $5 \mu\text{m}$ luminosity $3\times$ higher. Its luminosity probably exceeds the estimated $4 \times 10^{13} L_{\odot}$ of the most luminous obscured quasar in Polletta et al. (SWIRE J164216.93+410127.8; 2008), which has $4\times$ lower flux at $24 \mu\text{m}$. It approaches the $\sim 2 \times 10^{14} L_{\odot}$ of the most luminous known quasars such as S5 0014+813 (Kühr et al. 1983), HS 1700+6416 (Reimers et al. 1989), and SDSS J074521.78+473436.2 (Schneider et al. 2005). Several W1W2-dropouts reported in Wu et al. (2012) are even more luminous than WISE 1814+3412, with *minimum* L_{bol} up to $1.8 \times 10^{14} L_{\odot}$.

WISE 1814+3412 is also a massive, actively star forming LBG, with an extinction corrected UV star formation rate of $\sim 300 M_{\odot}\text{yr}^{-1}$ and a stellar mass of $\sim 3 \times 10^{11} M_{\odot}$ (several times the stellar mass of a field L^* galaxy today; Baldry et al. 2008). The specific star formation rate of $\sim 1 \text{ Gyr}^{-1}$ places WISE 1814+3412 in the starburst galaxy regime, but even the upper end of the extinction corrected UV SFR estimates account for $\lesssim 10\%$ of the bolometric luminosity. With no AGN signatures in the UV spectrum, it is tempting to assume that additional dust-obscured star formation accounts for the high bolometric luminosity. However, the upper limit at 1.1 mm would be greatly exceeded unless the star forming dust was significantly warmer than 35 K.

This possibility merits consideration. Kovács et al. (2006) present evidence that starburst dominated sub-millimeter galaxies have higher temperatures at higher redshifts and luminosities. The SED of the extreme low metallicity dwarf starburst galaxy SBS 0335-052 peaks at $30\mu\text{m}$ (Houck et al. 2004), and Hirashita & Hunt (2004) suggest that virtually all high redshift star formation may occur in the “active mode” for which SBS 0335-052 is the prototype. The active mode is characterized by dense, compact star-forming regions in which dust from core collapse SNe warms as it screens the gas from UV photons, enabling runaway star formation as the gas continues to cool on a dynamical timescale. Yet it is not obvious that this mechanism can be scaled up to the levels required to produce $\sim 10^{14} L_{\odot}$, i.e. a SFR $\sim 10^4 M_{\odot}\text{yr}^{-1}$ and $\sim 10^8$ O stars.

Since WISE 1814+3412 contains a modestly powerful radio source, an active galactic nucleus is almost certainly present. An obscured AGN powered by a super massive black hole (SMBH)

could supply the luminosity while being consistent with the absence of AGN signatures in the UV spectrum. In fact, despite the clear starburst signature from the optical spectrum, the lack of submm emission and predominance of hot dust suggest that in WISE 1814+3412 (and other W1W2-dropouts; Wu et al. 2012) we may be seeing an SED more like the “intrinsic” SED from the dusty central AGN region than is the case for many quasars (see Figure 6 of Netzer et al. 2007).

The formation and coevolution of AGN and stellar populations is the subject of much current research. Theoretical scenarios suggest the initial starburst rapidly enshrouds a forming galaxy in cold dust which emits at submm wavelengths. This is followed by an increase in fueling of the SMBH, triggering an AGN, generating warmer dust and mid-IR emission. Finally outflows from the AGN or starburst clear the dust and gas, revealing an optical quasar, and then removing the fuel which powers both starburst and quasar, leaving a quiescent massive galaxy (e.g., Sanders et al. 1988; Hopkins et al. 2006; Narayanan et al. 2009).

The black hole mass needed to power the bolometric luminosity is $2.8 \times 10^9 (L_{\text{Edd}}/L_{\text{bol}}) M_{\odot}$. But using the local $L_{\text{bulge}}/M_{\text{BH}}$ relation, the SED fit stellar component absolute magnitude of $M_K = -26.28$ gives a black hole mass of only $1.4 \times 10^9 M_{\odot}$ (Graham 2007). If the relation is actually between SMBH mass and bulge *mass* rather than bulge luminosity, as seems plausible, the discrepancy is larger. At $z = 2.452$ the stellar mass for a given K luminosity is likely less than half as large as today. Therefore, assuming the bolometric luminosity of the AGN template fit is correct, and that the Graham (2007) relation adjusted for lower $(M/L)_K$ at $z = 2.45$ applies, the implied Eddington ratio is $\gtrsim 4$. For comparison, Kollmeier et al. (2006) measure a typical Eddington ratio in luminous quasars of 0.25, and Kelly et al. (2010) find 0.1 to be representative. If WISE 1814+3412 has a similar Eddington ratio, then one of these assumptions does not hold.

The local stellar mass to SMBH mass relation could apply if the bolometric luminosity is mainly from star formation with warm dust similar to that in low metallicity starburst dwarf galaxies, but scaled up a factor of a thousand. There is evidence that starbursts can dominate luminosities even in sources with spectral signatures of quasars (e.g., Netzer et al. 2007; Polletta et al. 2008). Alternatively, the stellar mass may have been underestimated by a factor of several due to greater extinction at $4.5 \mu\text{m}$, but the extinction corrected stellar mass of $> 10^{12} M_{\odot}$ is then extreme. Note this argument holds for AGN with $L > 10^{14} L_{\odot}$ in general, and the largest SMBH masses in the most luminous objects may be well above the normal relation (e.g., McConnell et al. 2012; Salvander & Shields 2012). Another possibility is that WISE 1814+3412 is in an unstable transitional stage where the Eddington ratio is well above 1. Recently, Kawakatu & Ohsuga (2011) have argued that SMBH’s with super-Eddington accretion will be characterized by a low ratio of near-IR to bolometric luminosity, which is essentially the selection criterion for WISE 1814+3412.

We consider it more likely that WISE 1814+3412 lies well off the local M_{BH} -bulge mass relation, suggesting it may be in an early stage of its evolution where AGN activity is dominant and the object has yet to build the bulk of its stellar mass. This would, however, contradict the expectation that AGN activity should lag the peak of star formation (see e.g., Hopkins 2012). In

this context, the presence of 3 systems (components A, C, and D) at the same redshift and within 50 kpc suggests that a significant amount of stellar mass assembly lies in WISE 1814+3412’s future.

The authors thank Alex Pope for insightful discussions regarding the dust content of WISE 1814+3412; Alice Shapley for assistance in determining the star formation rate associated with a Lyman Break Galaxy; R. S. McMillan, J. V. Scotti, J. A. Larsen, and G. J. Bechetti for early ground-based followup observations; Conor Mancone for providing and answering questions about the convenient “Ez_Gal” web interface to the Bruzual-Charlot models; Leonidas Moustakas for suggesting references on the mass of L^* galaxies; Jeonghee Rho for allowing observations of WISE 1814+3412 during her CSO time; and Tom Soifer for allocating *Spitzer* Director’s Discretionary Time to observe WISE 1814+3412; and the anonymous referee for suggestions which improved the presentation of the paper.

R.J.A. and J.W. were supported by an appointment to the NASA Postdoctoral Program at the Jet Propulsion Laboratory, administered by Oak Ridge Associated Universities through a contract with NASA. NJE acknowledges support from NSF Grant AST-1109116. This publication makes use of data products from the Wide-field Infrared Survey Explorer, which is a joint project of the University of California, Los Angeles, and the Jet Propulsion Laboratory/California Institute of Technology, funded by the National Aeronautics and Space Administration. This work is based in part on observations made with the *Spitzer Space Telescope*, which is operated by the Jet Propulsion Laboratory, California Institute of Technology under contract with NASA. Some of the data presented here were obtained at the W.M. Keck Observatory, which is operated as a scientific partnership among Caltech, the University of California and NASA. The Keck Observatory was made possible by the generous financial support of the W.M. Keck Foundation. Some of the data are based on observations obtained at the Hale Telescope, Palomar Observatory as part of a continuing collaboration between the California Institute of Technology, NASA/JPL, and Cornell University. Some of the data presented here were obtained at the Kitt Peak National Observatory, National Optical Astronomy Observatory, which is operated by the Association of Universities for Research in Astronomy (AURA) under cooperative agreement with the National Science Foundation. The National Radio Astronomy Observatory is a facility of the National Science Foundation operated under cooperative agreement by Associated Universities, Inc.

Facilities: Wide-field Infrared Survey Explorer, *Spitzer Space Telescope* (IRAC) (MIPS), Palomar 200” (WIRC) (LFC), Keck (LRIS), Keck (NIRC2), KPNO (Mosaic), CSO (SHARC II) (Bolocam), EVLA, GBT

REFERENCES

- Assef, R. et al. 2010, ApJ, 713, 970
— . 2011, ApJ, 728, 56

- Baldry, I. K., Glazebrook, K., & Driver, S. P. 2008, *MNRAS*, 388, 945
- Bell, E. F., McIntosh, D. H., Katz, N., & Weinberg, M. D. 2003, *ApJS*, 149, 289
- Bennert, N., Falcke, H., Schulz, H., Wilson, A. S., & Wills, B. J. 2002, *ApJ*, 574, L105
- Blain, A. W., Chapman, S. C., Smail, I., & Ivison, R. 2004, *ApJ*, 611, 52
- Bochanski, J. J., West, A. A., Hawley, S. L., & Covey, K. R. 2007, *AJ*, 133, 531
- Bohlin, R. C., Savage, B. D., & Drake, J. F. 1978, *ApJ*, 224, 132
- Brand, K. et al. 2007, *ApJ*, 663, 204
- Bridge, C. et al. 2012, *ApJ*, submitted (arXiv: 1205.4030)
- Bruzual, G. & Charlot, S. 2003, *MNRAS*, 344, 1000
- Calzetti, D., Armus, L., Bohlin, R. C., Kinney, A. L., Koornneef, J., & Storchi-Bergmann, T. 2000, *ApJ*, 533, 682
- Cardelli, J. A., Clayton, G. C., & Mathis, J. S. 1989, *ApJ*, 345, 245
- Chabrier, G. 2003, *PASP*, 115, 763
- Cimatti, A., di Serego Alighieri, S., Vernet, J., Cohen, M., & Fosbury, R. A. E. 1998, *ApJ*, 499, L21
- Condon, J. J. 1992, *ARA&A*, 30, 575
- Condon, J. J., Cotton, W. D., Greisen, E. W., Yin, Q. F., Perley, R. A., Perley, G. B., Taylor, G. B., & Broderick, J. J. 1998, *AJ*, 115, 1693
- Cushing, M. C. et al. 2011, *ApJ*, 743, 50
- Desai, V. et al. 2006, *ApJ*, 641, 133
- Dey, A., Cimatti, A., van Breugel, W., Antonucci, R., & Spinrad, H. 1996, *ApJ*, 465, 157
- Dey, A. et al. 2008, *ApJ*, 677, 943
- Dowell, C. D. et al. 2003, *SPIE*, 4855, 73
- Eisenhardt, P. R., Armus, L., Hogg, D., Soifer, B. T., Neugebauer, G., & Werner, M. W. 1996, *ApJ*, 461, 72
- Feldman, G. J. & Cousins, R. D. 1998, *Phys. Rev. D*, 57, 3873
- Ferrarese, L. & Merritt, D. 2000, *ApJ*, 539, L9

- Floc'h, E. L. et al. 2005, *ApJ*, 632, L169
- Gebhardt, K. et al. 2000, *ApJ*, 539, L13
- Goodrich, R. W., Miller, J. S., Martel, A., Cohen, M. H., Tran, H. D., Ogle, P. M., & Vermeulen, R. C. 1996, *ApJ*, 456, L9
- Gordon, K. D. & Clayton, G. C. 1998, *ApJ*, 500, 816
- Graham, A. 2007, *MNRAS*, 379, 711
- Haig, D. J. et al. 2004, *SPIE*, 5498, 78
- Harrison, F. et al. 2010, *SPIE*, 7732, 27
- Hickox, R. C. et al. 2007, *ApJ*, 671, 1365
- Hill, R. J. et al. 2009, *ApJ*, 180, 246
- Hirashita, H. & Hunt, L. K. 2004, *A&A*, 421, 555
- Hopkins, A. M. 2004, *ApJ*, 615, 209
- Hopkins, P. F. 2012, *MNRAS*, 420, L8
- Hopkins, P. F., Hernquist, L., Cox, T. J., Matteo, T. D., Robertson, B., & Springel, V. 2006, *ApJS*, 163, 1
- Houck, J. R. et al. 2004, *ApJS*, 154, 211
- Ibata, R. A., Lewis, G. F., Irwin, M. J., Lehár, J., & Totten, E. J. 1999, *AJ*, 118, 1922
- Iverson, R. J. et al. 2010, *A&A*, 518, L31
- Kawakatu, N. & Ohsuga, K. 2011, *MNRAS*, 417, 2562
- Kelly, B. C., Vestergaard, M., Fan, X., Hopkins, P., Hernquist, L., & Siemiginowska, A. 2010, *ApJ*, 719, 1315
- Kennicutt, R. C. 1998, *ARA&A*, 36, 189
- Kirkpatrick, J. D. et al. 2011, *ApJS*, 197, 19
- Kollmeier, J. A. et al. 2006, *ApJ*, 648, 128
- Kovács, A. 2006, PhD thesis, Caltech
- Kovács, A., Chapman, S. C., Dowell, C. D., Blain, A. W., Iverson, R. J., Smail, I., & Phillips, T. G. 2006, *ApJ*, 650, 592

- Kuhr, H., Liebert, J. W., Strittmatter, P. A., Schmidt, G. D., & Mackay, C. 1983, *ApJ*, 275, L33
- Leong, M., Peng, R., Houde, M., Yoshida, H., Chamberlin, R., & Phillips, T. G. 2006, *SPIE*, 6275, 21
- Magorrian, J. et al. 1998, *AJ*, 115, 2285
- Mainzer, A. et al. 2011a, *ApJ*, 726, 30
- . 2011b, *ApJ*, 731, 53
- Maiolino, R., Marconi, A., Salvati, M., Risaliti, G., Severgnini, P., Oliva, E., Franca, F. L., & Vanzani, L. 2001, *A&A*, 365, 28
- Mason et al. 2009, *ApJ*, 704, 1433
- Massey, P. & Gronwall, C. 1990, *ApJ*, 358, 344
- McConnell, N. J., Ma, C.-P., Murphy, J. D., Gebhardt, K., Lauer, T. R., Graham, J. R., Wright, S. A., & Richstone, D. O. 2012, *ApJ*, submitted (astro-ph/1203.1620)
- Narayanan, D., Cox, T. J., Hayward, C. C., Younger, J. D., & Hernquist, L. 2009, *MNRAS*, 400, 1919
- Nenkova, M., Sirocky, M. M., Nikutta, R., Ivezić, Ž., & Elitzur, M. 2008, *ApJ*, 685, 160
- Netzer, H. et al. 2007, *ApJ*, 666, 806
- Oke, J. B. et al. 1995, *PASP*, 107, 375
- Patten, B. M. et al. 2006, *ApJ*, 651, 502
- Polletta, M., Weedman, D., Hönligh, S., Lonsdale, C. J., Smith, H. E., & Houck, J. 2008, *ApJ*, 675, 960
- Reimers, D., Clavel, J., Groote, D., Engels, D., Hagen, H. J., Naylor, T., Wamsteker, W., & Hopp, U. 1989, *A&A*, 218, 71
- Richards, G. T. et al. 2006a, *AJ*, 131, 2766
- . 2006b, *ApJS*, 166, 470
- Salviander, S. & Shields, G. A. 2012, *AAS Abstracts*, 219, 435.03
- Sandell, G. 1994, *MNRAS*, 271, 75
- Sanders, D. et al. 1988, *ApJ*, 325, 74
- Sawyer, D. G., Daly, P. N., Howell, S. B., Huntten, M. R., & Schweiker, H. 2010, *SPIE*, 7735, 111

- Sayers, J., Golwala, S. R., Ameglio, S., & Pierpaoli, E. 2011, *ApJ*, 728, 39
- Sayers, J. et al. 2009, *ApJ*, 690, 1597
- Schneider, D. P. et al. 2005, *AJ*, 130, 367
- Shapley, A. E., Steidel, C. C., Pettini, M., & Adelberger, K. L. 2003, *ApJ*, 588, 65
- Simcoe, R. A., Metzger, M. R., Small, T. A., & Araya, G. 2000, *BAAS*, 32, 758
- Stern, D., Djorgovski, S. G., Perley, R., de Carvalho, R., & Wall, J. 2000, *AJ*, 132, 1526
- Stern, D. et al. 2005, *ApJ*, 631, 163
- Weedman, D. et al. 2006, *ApJ*, 653, 101
- Wilson, J. C. et al. 2003, *SPIE*, 4841, 451
- Wizinowich, P. L. et al. 2006, *PASP*, 118, 297
- Wright, E. L. et al. 2010, *AJ*, 140, 1868
- Wu, J. et al. 2012, *ApJ*, 756, 96

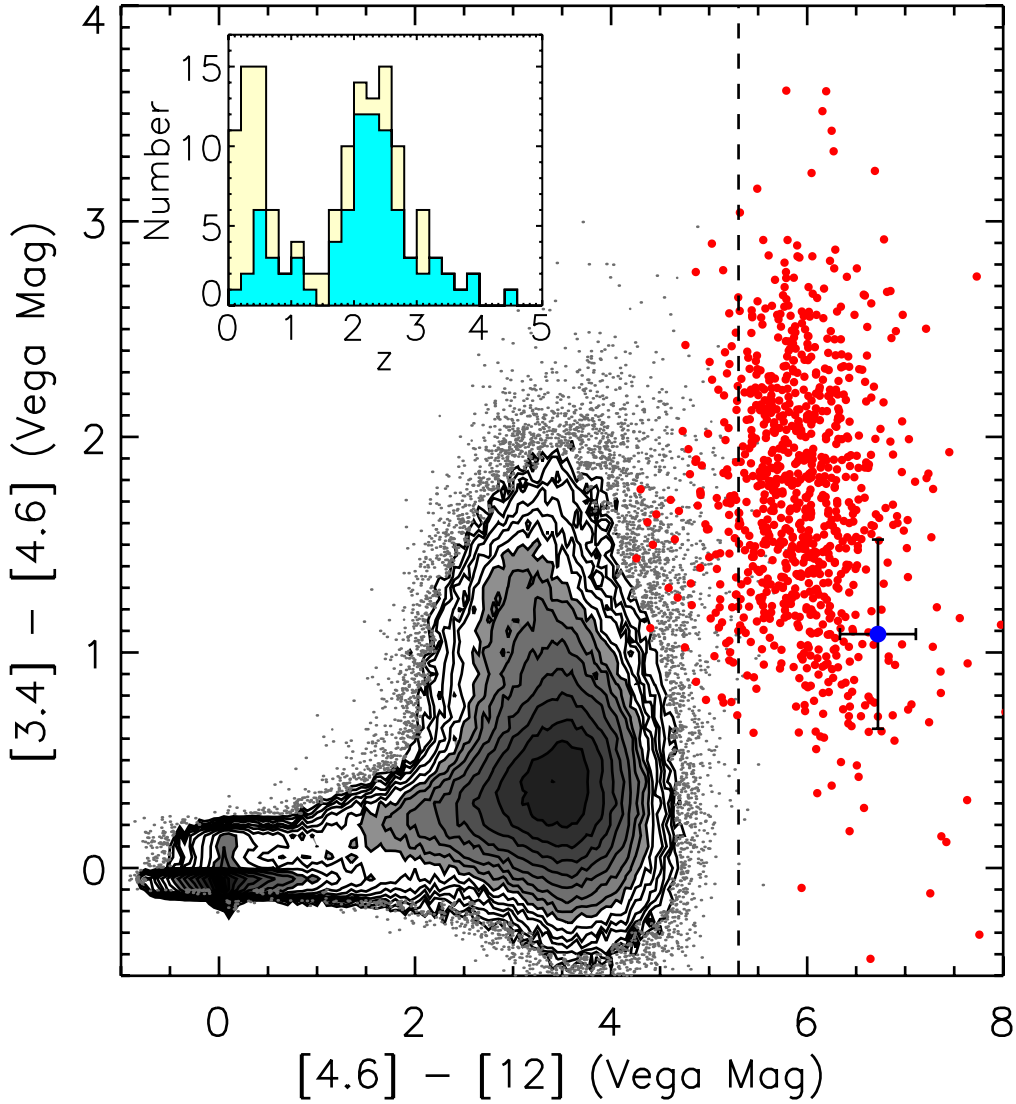


Fig. 1.— WISE color-color plot of the 226,017 sources with < 0.3 mag errors in W1 ($3.4 \mu\text{m}$), W2 ($4.6 \mu\text{m}$), and W3 ($12 \mu\text{m}$), in the 313.4 square degree area of the all-sky release catalog with Galactic latitude $b > 80^\circ$ (black points and gray regions). These represent about 8% of all WISE catalog sources in this region. The larger red points are for 907 W1W2-dropouts selected over the whole sky, excluding the Galactic plane and bulge, an area ~ 100 times larger, illustrating the rarity of the W12drop population. The inset shows the histogram of available redshifts for the W12drop sample, with the cyan shading corresponding to W1W2-dropouts not seen in the optical digitized sky survey. The contours are in surface density at power law steps of $\sqrt{2}$, with the outermost contour at 10 sources per $0.05 \text{ mag} \times 0.05 \text{ mag}$. The colors plotted for the W1W2-dropouts use *Spitzer* 3.6 and $4.5 \mu\text{m}$ followup data since they are generally not detected at 3.4 and $4.6 \mu\text{m}$ by WISE. *Spitzer* data were converted to the WISE system using $[3.4] - [4.6] = W1 - W2 = 1.4([3.6] - [4.5])$, and $[4.6] - [12] = W2 - W3 = 0.07 + [4.5] - [12]$. The large blue symbol with error bars is for WISE 1814+3412. The vertical dashed line at $W2 - W3 = 5.3$ is one of the selection criteria for W1W2-dropouts; some are bluer than this because they satisfied the $W2 - W4 > 8.2$ criterion.

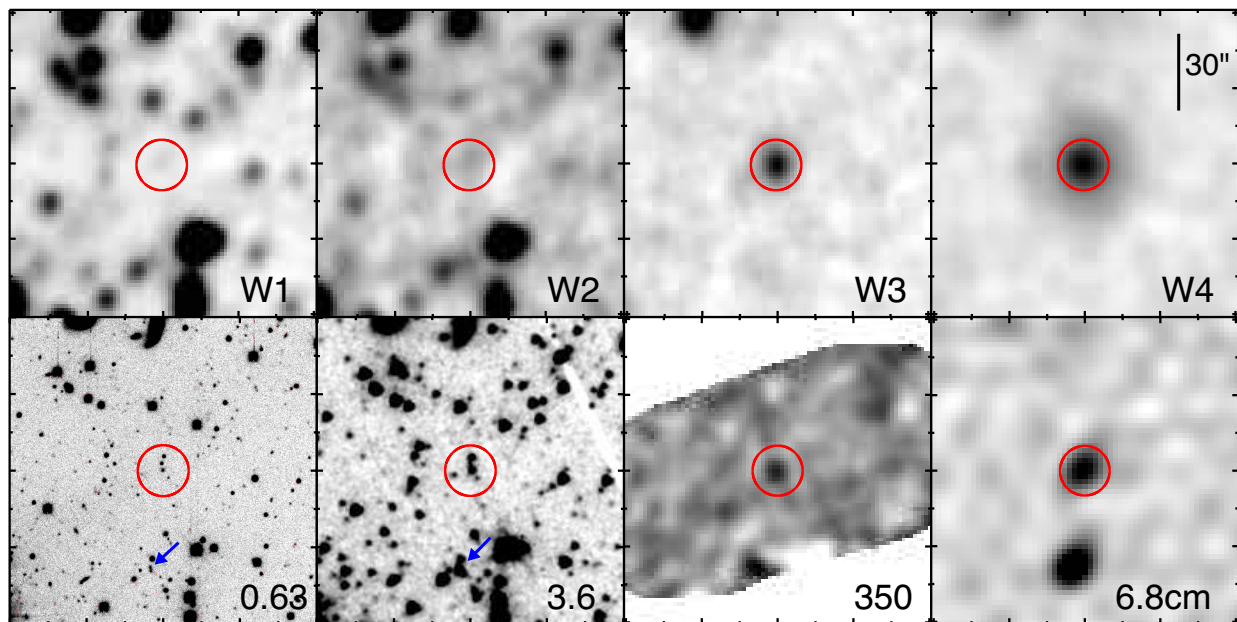


Fig. 2.— Top row: Images of WISE 1814+3412 in the WISE W1 ($3.4 \mu\text{m}$), W2 ($4.6 \mu\text{m}$), W3 ($12 \mu\text{m}$), and W4 ($22 \mu\text{m}$) bands, from left to right. Second row: Followup images at r' ($0.63 \mu\text{m}$), $3.6 \mu\text{m}$, $350 \mu\text{m}$, and 4.5 GHz (6.8 cm), from left to right. Images are 2 arcmin on a side, with North up and East to the left. Circles are $10''$ in radius, centered on the WISE source position. The counterpart to the southern radio source apparent in the 6.8 cm image is indicated with a blue arrow in the $0.63 \mu\text{m}$ and $3.6 \mu\text{m}$ images.

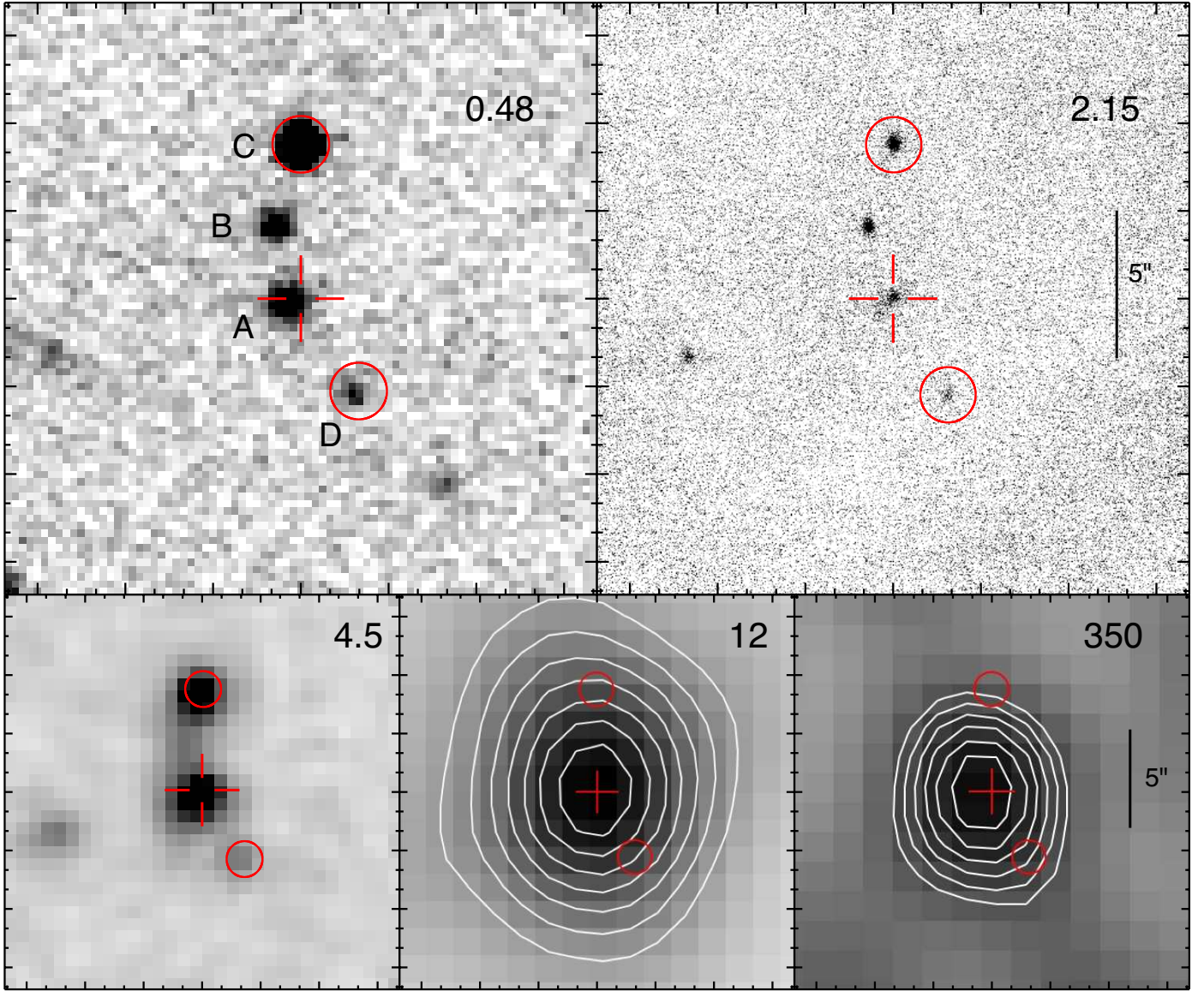


Fig. 3.— Images of the region near WISE 1814+3412 in g' ($0.48 \mu\text{m}$ - top left), K_s ($2.15 \mu\text{m}$ - top right), $4.5 \mu\text{m}$ - bottom left, W3 ($12 \mu\text{m}$ - bottom center), and $350 \mu\text{m}$ (bottom right). The field is $20''$ on a side with North up and East left. Component A is resolved in the g' and K_s images, while B and C are unresolved. Components A and D show a Lyman-break galaxy spectrum at $z = 2.45$, component C is a broad-lined quasar at $z = 2.45$, and component B is an M-dwarf star. The relative position in the K_s image of component A with respect to component C is marked with red cross-hairs, showing that component A is displaced $\sim 0''.5$ East in the g' image. Contours at 12 and $350 \mu\text{m}$ are from 30 to 90% of the peak in each image. The emission at 12 and $350 \mu\text{m}$ is dominated by and centered on component A to within the astrometric errors, implying that the other $z = 2.45$ components (C and D, whose locations are marked with circles) make little contribution to the bolometric luminosity.

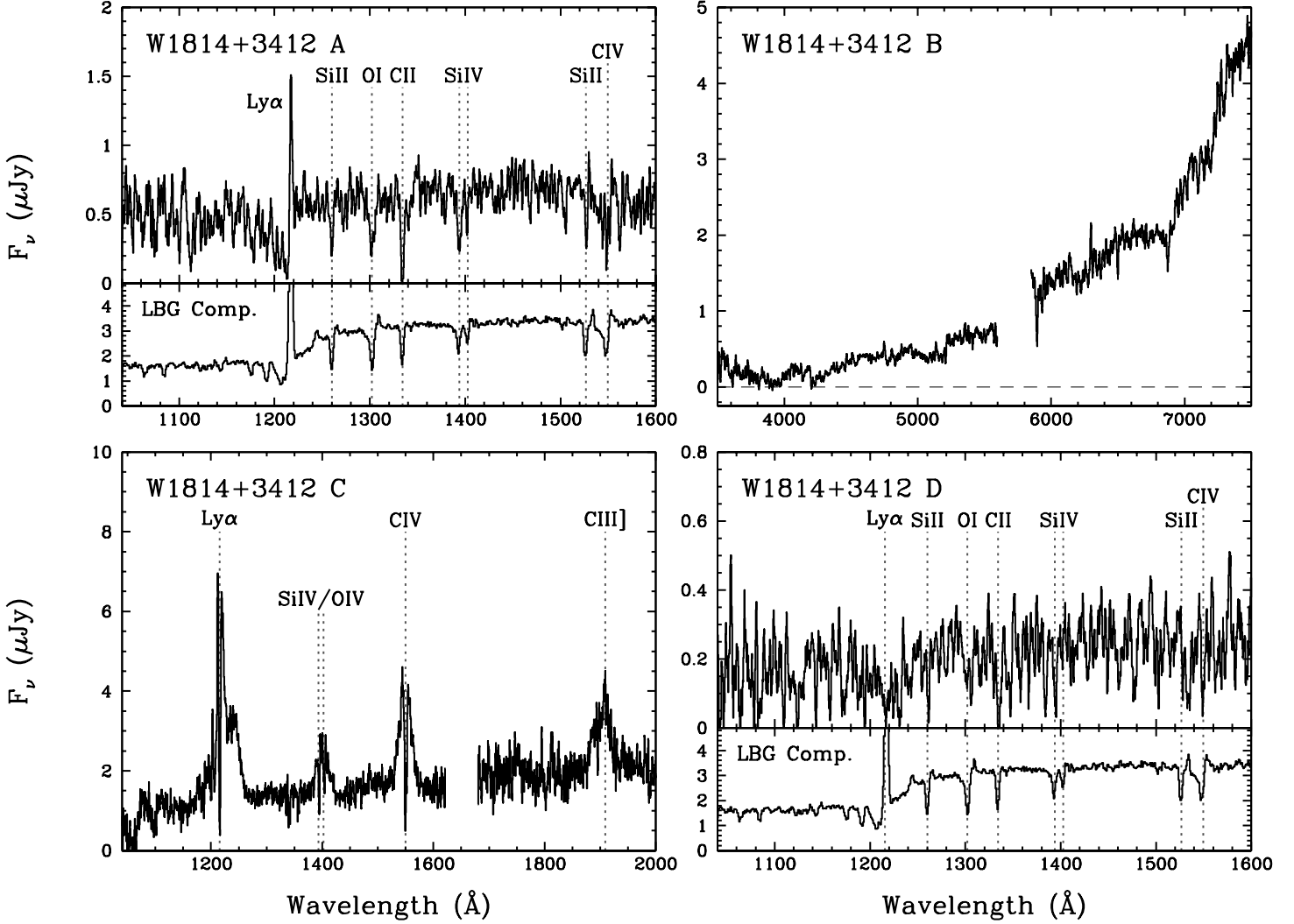


Fig. 4.— Keck/LRIS spectra of optical components near WISE 1814+3412, as marked in the upper left panel of Figure 3. Upper left: Component A, shifted to the rest frame for $z = 2.452$. The composite rest-frame ultraviolet spectrum of $z \sim 3$ LBGs from Shapley et al. (2003) is shown directly below for comparison. Upper right: Component B spectrum in the observed frame. This is an optically red point source with spectrum and photometry consistent with an M-dwarf star. Lower left: Component C in the rest frame for $z = 2.452$, showing a bright quasar with narrow self-absorption at the same redshift as WISE 1814+3412. Lower right: Component D in the rest frame for $z = 2.452$. The broad Ly α absorption, continuum break, and detection of several interstellar absorption lines imply that component D is at the same redshift as WISE 1814+3412. The Shapley et al. (2003) composite LBG spectrum is again shown directly below for comparison.

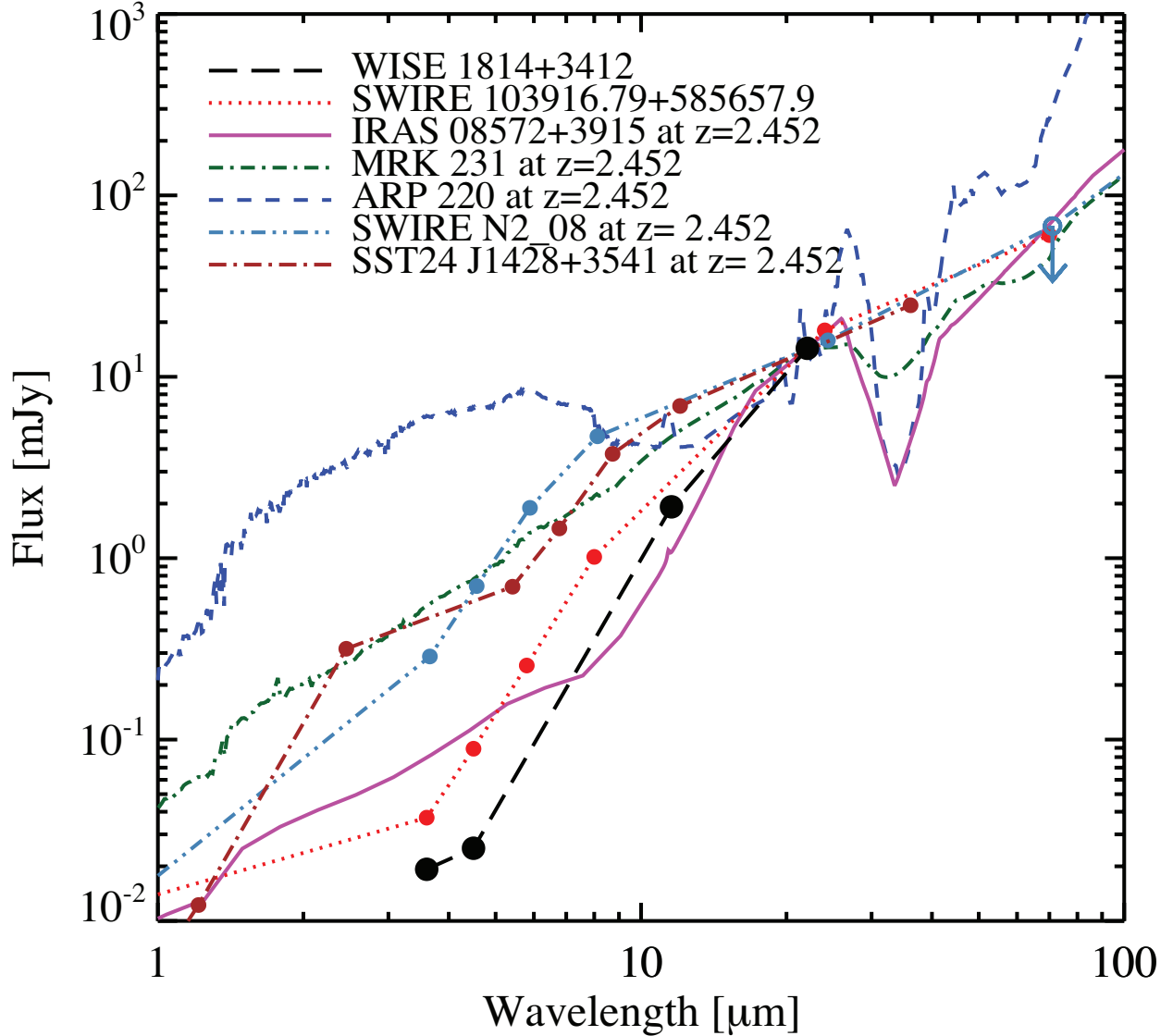


Fig. 5.— *Spitzer* photometry at 3.6 and 4.5 μm and WISE photometry at 12 and 22 μm for WISE 1814+3412, compared to SED’s of other unusually red objects whose wavelengths have been scaled to $z = 2.452$ and flux densities scaled to the 22 μm flux density of WISE 1814+3412. The approximate flux density scaling factors and observed redshifts are: SWIRE J103916.79+585657.9 (4, z unknown but assumed to be 2.452, Weedman et al. 2006); IRAS 08572+3915 (0.06, $z = 0.058$); Mrk 231 (0.02, $z = 0.042$); Arp 220 (0.05, $z = 0.018$); SWIRE N2_08 (SWIRE J164216.93+410127.8, 4, $z = 2.40$, Polletta et al. 2008); and SST24 J1428+3541 (2.3, $z = 1.293$, Desai et al. 2006).

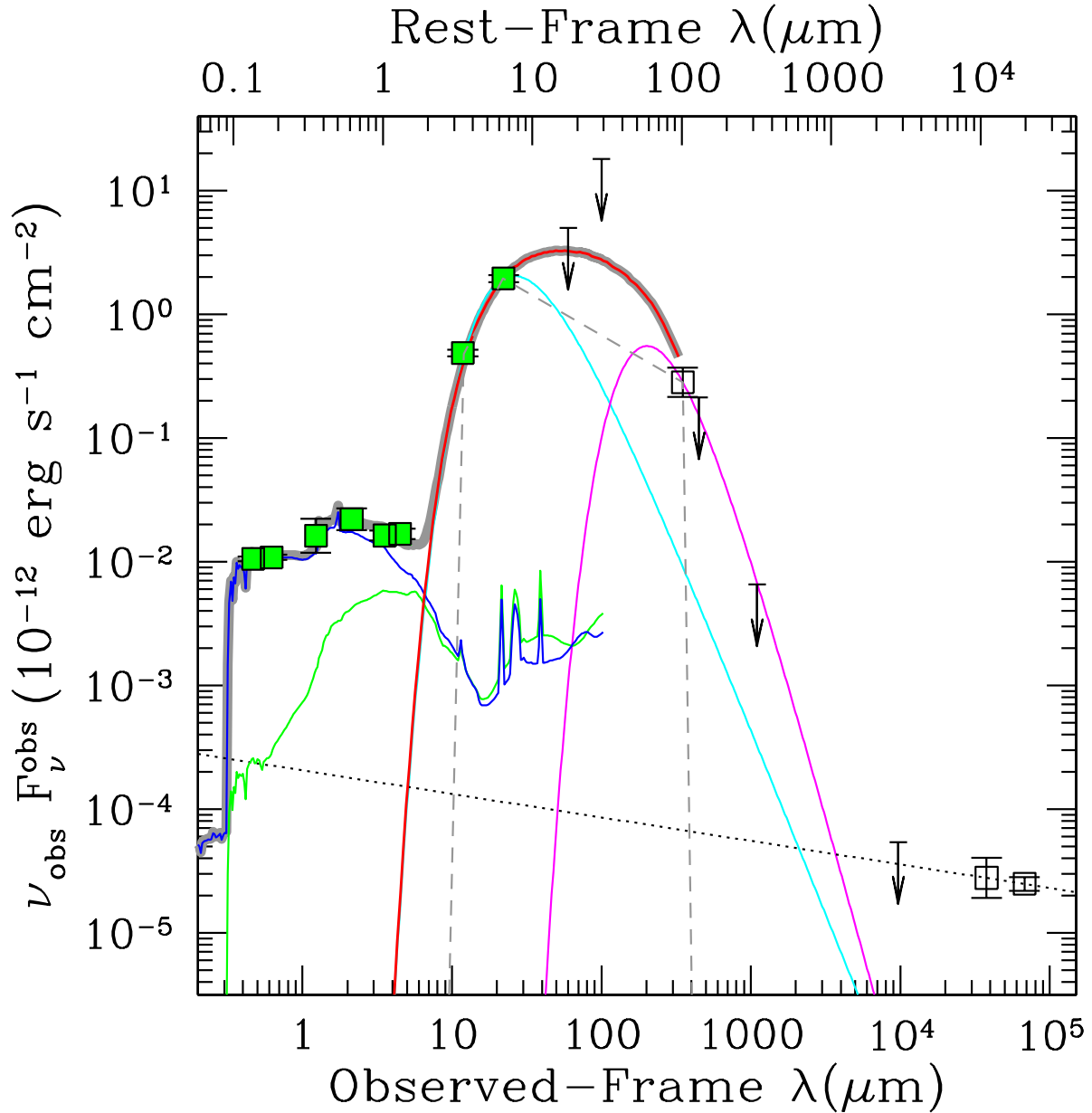


Fig. 6.— Best fit SED template model (heavy grey line) to the photometry (shown by green symbols) for WISE 1814+3412 plotted in νF_ν units. Other measurements (black symbols) and upper limits (black downward pointing arrows) were not used for the template fit. The template fit uses starburst (blue) and Sbc spiral (green) components from Assef et al. (2010), and the Richards et al. (2006b) Type I AGN template (red) with $A_V = 48$ extinction applied. The cyan line shows a 488 K blackbody fit to the W3 (12 μm) and W4 (22 μm) photometry which overlaps the red curve below 12 μm , while the magenta line shows a modified (i.e., with dust emissivity $\propto \nu^{1.5}$) 45 K blackbody fit to the 350 μm flux density and the upper limit at 1.1 mm. The dotted line shows an $F_\nu \propto \nu^{-0.8}$ power law fit to the radio data. The grey dashed line shows the power laws used to estimate the minimum bolometric luminosity in §3.2.

Table 1. Photometry for WISE 1814+3412

Band	$\lambda(\mu\text{m})$	Instrument	Flux Density (μJy)	Comp. B (μJy)
g'	0.48	MOSAIC	1.64 ± 0.074	0.81 ± 0.030
r'	0.63	MOSAIC	2.25 ± 0.11	3.16 ± 0.063
J	1.25	NIRC2	6.6 ± 2.1	14.0 ± 3.0
K_s	2.15	NIRC2	15.7 ± 3.2	10.9 ± 2.2
[3.6]	3.6	IRAC	19.3 ± 1.9	5.06 ± 0.49
[4.5]	4.5	IRAC	25.2 ± 2.4	3.77 ± 0.39
W3	12	WISE	1860 ± 100	
W4	22	WISE	14380 ± 870	
	60	IRAS	< 100000	
	100	IRAS	< 600000	
	350	SHARC-II	33000 ± 9000	
	450	SHARC-II	< 35000	
	1100	Bolocam	< 2400	
Ka	9700	GBT	< 175	
C-band high	37800	EVLA	350 ± 130	
C-band low	67700	EVLA	560 ± 70	

Table 2. Astrometry for WISE 1814+3412

Band	RA (J2000.0)	Decl. (J2000.0)	RA B	Decl. B	RA C	Decl. C	RA D	Decl. D
g'	18 14 17.32 \pm 0.02	34 12 24.9 \pm 0.2	17.34	27.6	17.28	30.3	17.13	21.9
r'	18 14 17.31 \pm 0.02	34 12 25.1 \pm 0.2	17.34	27.6	17.27	30.4	17.14	21.8
J	18 14 17.29 \pm 0.02	34 12 25.2 \pm 0.2	17.35	27.6	17.27	30.5		
K_s	18 14 17.27 \pm 0.02	34 12 25.3 \pm 0.2	17.34	27.7	17.27	30.5	17.12	22.0
[3.6]	18 14 17.29 \pm 0.02	34 12 25.1 \pm 0.2	17.35	27.6	17.28	30.2	17.13	21.9
[4.5]	18 14 17.29 \pm 0.02	34 12 25.1 \pm 0.2	17.33	27.7	17.29	30.2	17.13	22.0
WISE	18 14 17.30 \pm 0.02	34 12 25.0 \pm 0.3						
350 μm	18 14 17.31 \pm 0.20	34 12 25.5 \pm 2.0						
C-band high	18 14 17.26 \pm 0.05	34 12 24.2 \pm 1.2						
C-band low	18 14 17.33 \pm 0.03	34 12 24.9 \pm 0.5						